The 2002/2003 El Nino: Equatorial waves sequence and their impact on sea surface temperature

K. Mosquera-Vasquez, B. Dewitte, S. Illig, K. Takahashi, G. Garric

The 2002/2003 El Niño: Equatorial waves sequence and their impact on sea surface temperature

K. Mosquera-Vásquez,[1,2] B. Dewitte,[1,2] S. Illig,[1,2] K. Takahashi,[1] and G. Garric[3]

Received 25 September 2012; revised 30 November 2012; accepted 3 December 2012.

[1] The recent decades have experienced changes in the characteristics of the El Niño phenomenon, with in particular an increased occurrence of so-called Modoki or Central Pacific El Niños. Here the 2002/2003 El Niño, characterized as a Central Pacific El Niño, is studied from an Ocean General Circulation Model simulation. The focus is on the sequence of equatorial waves and their impact on zonal and vertical advection. The wave amplitude according to the most energetic baroclinic modes are first estimated, which allows inferring the sequence of the intraseasonal equatorial Kelvin (IKW) and Rossby (IRW) waves. It is shown that energetic downwelling IKWs, forced in the western-central Pacific, crossed the equatorial Pacific. Reflections of IKWs into IRWs onto the zonally varying thermocline and eastern boundary are also observed. A simplified heat budget of the surface layer is then carried out to infer the dominant processes at work during the evolution of this event focusing on the wave-induced advection terms. The results indicate that the warming phase (April–November 2002) is mainly controlled by zonal advection of mean temperature (accounted for by IKWs and locally wind-driven current) and by vertical advection in the eastern Pacific. The cooling phase (December 2002 to April 2003) is dominated by a reduction in solar radiation and the IRW-induced zonal advection of mean temperature respectively in the central and eastern equatorial Pacific. The recharge-discharge process is also showed to be at work with the recharge (discharge) process operating mainly through the second (first) baroclinic mode.

Citation: Mosquera-Vásquez, K., B. Dewitte, S. Illig, K. Takahashi, and G. Garric (2013), The 2002/2003 El Niño: Equatorial waves sequence and their impact on sea surface temperature, *J. Geophys. Res. Oceans*, *118*, doi:10.1029/2012JC008551.

1. Introduction

[2] The first El Niño of the 21st century took place in 2002/2003 and has been categorized for the scientific community as a Central Pacific El Niño (hereafter CP El Niño) or Modoki El Niño. CP El Niño consists in a warming of the sea surface temperature (SST) in the central Pacific that is larger than the one occurring in the eastern Pacific at the peak phase of the event, namely in December-January-February (DJF) [*Ashok et al*., 2007; *Kug et al*., 2009; *Yeh et al*., 2009]. The occurrence of CP El Niño has increased in the recent decades [*Lee and McPhaden*, 2010; *Yeh et al*., 2009] and the last 10 years has witnessed only El Niño events of this type, which has drawn the interest of the community in its dynamics and predictability [*Ashok et al*., 2007]. *Kug et al*. [2009] tested the recharge-discharge process [*Jin*, 1997] that applies for the so-called eastern Pacific (hereafter EP El Niño) to this type of event based on a reanalysis product. They conclude that the discharge process of the equatorial heat content associated with the CP El Niño is not efficient owing to the spatial structure of SST anomaly. They also show from composite analysis that the zonal advective feedback (i.e., zonal advection of mean SST by anomalous zonal currents) plays a crucial role in the development of a decaying SST anomaly associated with the CP El Niño, while the thermocline feedback is a key process during the EP El Niño. Despite this contrasted feature in the dynamics of the CP and EP events, the classification of the El Niño into two types may still be oversimplified. In fact *Kug et al*. [2009] introduced three types of El Niño, i.e., CP, EP, and a mixed type, which corresponds to SST anomalies peaking in the NINO34 region (5°S–5°N; 170°W–120°W). For instance, the last El Niño to date that took place in 2009–2010 can be categorized as a CP El Niño [*Kim et al*., 2011] but its ocean dynamical behavior resembles the EP El Niño. *Yu et al*. [2011] also propose to define CP El Niño and mixed-type El Niño based on subsurface indices that are more appropriate to capture the specificities of the events and account for the larger diversity of the El Niño types in nature than what is generally simulated in models [*Yu and Kim*, 2010; *Kug et al*., 2010; *Dewitte et al*., 2012]. *Takahashi et al*. [2011] somehow reconciles these studies proposing to classify the El Niño event according to their

[1]Instituto Geofísico del Perú (IGP), Calle Badajoz N° 169-171, Urbanización Mayorazgo, IV Etapa, Lima 3, Perú.
[2]LEGOS, 18, av. Edouard Belin, 31401, Toulouse cedex 9, France.
[3]MERCATOR, 8-10 rue Hermès, 31520, Ramonville St-Agne, France.

Corresponding author: K. Mosquera-Vásquez, Instituto Geofísico del Perú (IGP), Calle Badajoz N° 169–171, Urbanización Mayorazgo, IV Etapa, Lima 3, Perú. (kobi.mosquera@igp.gob.pe)

2169-9275/13/2012JC008551

privileged regimes defined in their study from the first two principal component time series of the SST anomalies in the tropical Pacific. In particular, the mixed-type El Niño of *Kug et al*. [2009] fits perfectly with the so-called C regime of *Takahashi et al*. [2011] in terms of its spatial pattern, which suggests that within a regime, El Niño event can have in fact a different dynamics. A dynamically based classification of the El Niño event is probably required, which implies documenting the balance between processes controlling the rate of SST changes in the equatorial Pacific during the evolution of these types of El Niño events. This study lies into this line of research focusing on the 2002/2003 El Niño, a CP El Niño according to current definitions [*Yeh et al*., 2009; *Takahashi et al*., 2011]. As an illustration, Figure 1 presents the evolution of the observed SST, sea surface height (SSH), 20°C isotherm depth anomalies over two different regions along the equator and along the coast of Peru. Along the equator, the 2002/2003 El Niño is characterized by a comparable warming of the NINO3 (150°W–90°W; 5°S–5°N) and NINO4 (150°E–150°W; 5°S–5°N) regions of the order of 1°C. However, whereas during the developing phase, the NINO3 index is above the NINO4 index, at the peak phase (December–January-February season) the warming in the western Pacific is slightly larger, which implies its central Pacific-type following *Yeh et al*. [2009]. As a consistency check of the nature of this El Niño event, we verify that it belongs to the C regime defined by *Takahashi et al*. [2011]: Figure 1d presents the evolution of these indices over the period of interest (based on HadISST data [*Rayner et al*., 2003]). It shows that the *C* index is positive with values above its standard deviation where the *E* index is mostly negative except around November 2002 when it peaks to ~0.8°C. Clearly, the 2002/2003 El Niño belongs to the *C* regime but it also evidences some contribution from the *E* regime, which reflects its mixed nature. Interestingly, this CP El Niño is also associated to pulses of warm SST anomalies

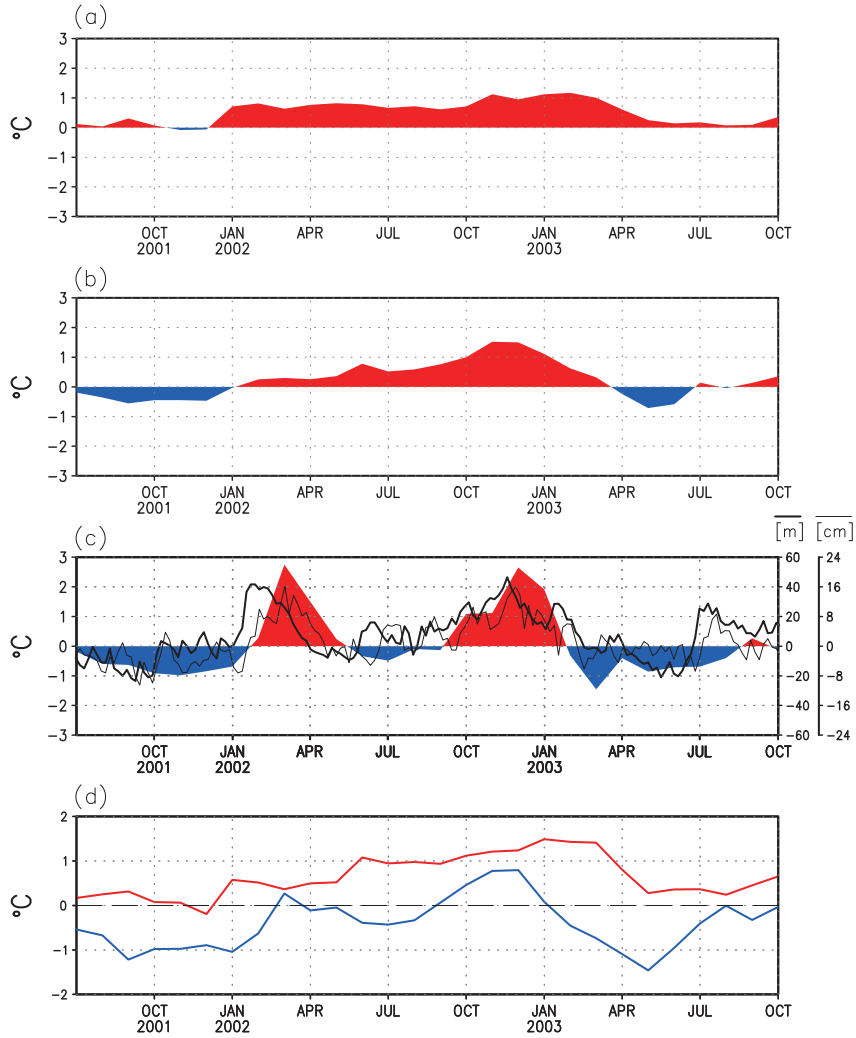

Figure 1. Time series for the period July 2001 to October 2003. Bicolor (red/blue) filled plot represents the TMI's SST anomaly for (a) NINO4 (150°E–150°W; 5°S–5°N), (b) NINO3 (150°W–90°W; 5°S–5°N), and (c) *Puerto Chicama* coastal station (Courtesy of IMARPE). In Figure 1c, thick (thin) black line indicates the 20 °C isotherm depth (sea level height) anomaly, in meters (centimeters), from TAO Project (Lobos de Afuera coastal station located at the Peruvian coast) at the equator (6°56′S) and 110°W (80°43′W). (d) The *C* (red) and *E* (blue) indices as defined in *Takahashi et al*. [2011]. Anomalies are relative to the climatology over 2000–2008 for Figures 1a,1b, and 1c and over 1958–2008 for Figure 1d.

near the coast of Peru (Figure 1c) that may correspond to the arrivals of downwelling Kelvin waves at the Ecuadorian coast (Figure 1c), as suggested by the good correspondence of the SST anomalies at Chicama (8°S) and either the 20°C isotherm depth anomaly at 110°W or the sea level anomalies at Lobos de Afuera coastal station (Figure 1d). These perturbations observed at the coast suggest their intraseasonal nature because there is no corresponding anomalies of the NINO3 index and intraseasonal equatorial Kelvin wave are theoretically trapped at these frequencies [*Clarke and Shi*, 1991]. It indicates that the 2002/2003 El Niño was associated to energetic equatorial wave forcing. Still, the 2002/2003 El Niño, the first El Niño of this century, was very different from its predecessor in terms of magnitude, evolution and teleconnection [*McPhaden*, 2004]. *McPhaden* [2004] provided a comprehensive description of the evolution of this unusual event from the TAO array data and satellite observations. Whereas this event gathered some ingredients of the canonical El Niño-Southern Oscillation (ENSO), namely a build-up in heat content along the equator two to three seasons prior to its onset as well as strong Madden-Julian Oscillation related westerly winds prior to the peak phase, it was surprisingly weaker than the 1997/1998 El Niño. This was argued to be the results of processes (not identified) counteracting the tendency for remote forcing to deepen the thermocline in the eastern basin, leading to weaker SST anomalies that would have been expected there. The resulting anomalous zonal SST contrast suggests that the large-scale ocean-atmosphere feedbacks may not have fully engaged to amplify and sustain the El Niño warming. On the other hand, episodic westerlies, particularly that are related to the Madden-Julian Oscillation, may have participated to the persistence of warm anomalies in the central Pacific through the forcing of downwelling Kelvin waves. As pointed out by *McPhaden* [2004], a better understanding of the factors giving rise to the unusual SST pattern of the 2002/2003 El Niño requires a quantitative evaluation of the processes from a coupled ocean-atmosphere perspective. This is the objective of this paper that focuses on the analysis of the equatorial Kelvin waves and their contribution to the main ENSO feedback processes, namely the zonal advective feedback and the thermocline feedback. In particular, we use an OGCM (Ocean General Circulation Model) simulation to carry out a heat budget of the evolution of the 2002/2003 El Niño, highlighting the contribution of locally and remotely forced variability to the advection terms. The proposed analysis is aimed at providing material for the interpretation of evolution of this event in the light of current ENSO theories, and in particular the recharge-discharge mechanism [*Jin*, 1997].

[3] The paper is organized as follows: Section 2 describes the data sets, the model, and the methods. Section 3 provides a description of the wave sequence during the 2002/2003 El Niño and then analyzes the results of a simplified heat budget model during the different phases of the event. Section 4 is a discussion followed by concluding remarks.

2. Data and Methods Description

[4] The study is based on the analysis of an OGCM simulation over the period 2000–2008 that was previously validated from in situ and satellite observations (see section 2.4). The mean circulation and intraseasonal to interannual variability (anomalies) of the model are considered. Anomalies are calculated as the deviation from the mean seasonal cycle over the period 2000–2007. The seasonal cycle is derived from the monthly mean of the data, which is then interpolated on a 3 day mean temporal grid using spline functions. The seasonal cycle was smoothed with a 1-2-1 filter before calculating anomalies. The same postprocessing is performed for all data sets used in this study.

2.1. Temperature and Zonal Currents From TAO

[5] In situ temperature and current data from the Tropical Atmosphere Ocean (TAO) project array [*Hayes et al*., 1991; *McPhaden et al*., 1998] were used in this study for validating the model skills along the equator (see section 2.4). Vertical profiles of zonal current data from equatorial TAO moorings are considered at four sites: 147°E, 165°E, 140°W, and 110°W, whereas temperature data are taken at the 10 TAO mooring sites (147°E, 156°E, 165°E, 180°, 170°W, 155°W, 140°W, 125°W, 110°W and 95°W). The last group is used to derive the depth of the 20°C isotherm that is taken as a proxy for the thermocline depth. Daily current and temperature data were averaged into 3 day mean to compare with model outputs.

2.2. Sea Surface Temperature From Tropical Rainfall Measuring Mission Microwave Imager

[6] The 3 day mean SST data as derived from the Tropical Rainfall Measuring Mission Microwave Imager (TMI) (*Wentz et al*. [2000], http://www.remss.com/) is compared to the output model temperature at 0.49 m (the first vertical level) along the equatorial line. The estimated SST is based mainly on emissions at 10.7 GHz, and is also largely uninfluenced by cloud cover, rain, aerosols and atmospheric water vapor [*Wentz et al*., 2000]. However, the microwave retrievals are sensitive to (wind-induced) sea-surface roughness. TMI comparisons with buoys give an RMS error of about 0.6 K [*Wentz et al*., 2000] due to a combination of instrumental (buoy) collocation error [*Gentemann et al*., 2003]. Comparisons of the TMI SST product with buoy-measured near-surface ocean temperature show that, on greater than weekly time scales, TMI SST reproduces the characteristics of the 1 m buoy-observed temperatures in the tropical Pacific [*Chelton et al*., 2001].

2.3. Sea Level Height From Merged Product TOPEX-POSEIDON/JASON

[7] The gridded sea level anomaly data were supplied by AVISO/altimetry [*Ducet et al*., 2000]. They were built by optimal interpolation of *T*/*P* and ERS data on a 1/4° × 1/4° grid every 10 days. If a precision of individual instantaneous measurements is of order of 6 cm RMS [*Fu et al*., 1994], errors on such gridded data is estimated to 2–3 cm RMS for 10 day map and spatial scales of order of 200 km and more [*Le Traon and Ogor*, 1998].

2.4. OGCM Simulation

[8] The outputs of the MERCATOR global OGCM (http://www.mercator-ocean.fr/html/produits/index_en.html) are used. MERCATOR is an eddy-permitting ¼° model, based on the primitive-equation global ocean general circulation model Océan PArallélisé [*Madec et al*., 1998] and developed

at the Laboratoire d'Océanographie et du Climat: Expérimentations et Approches Numériques. The model was forced with daily surface atmospheric conditions from the European Center for Medium Range Weather Forecast Integrated Forecast System analysis. The simulation is hereafter referred to as MERCATOR (see *Garric et al*. [2008] for more details). Here the experiment was initialized on 4 April 1998 with an ocean at rest and climatologic temperature and salinity from *Levitus et al*. [1998] data set. Three key fields were analyzed for the model validation: (1) the mean SST and its variability, (3) the mean thermocline depth and its variability, and (3) the sea level variability. Figure 2 presents the results of the comparison between observations and the simulation for these different fields along the equatorial line. It indicates that the model is skillful in capturing most aspects of the observed variability. In particular, the thermocline variability along the equator is rather realistic with correlation between model and observations reaching 0.76 on average along the equator. Such skill is comparable to other Reanalysis products like Simple Ocean Data Assimilation or Global Ocean Data Assimilation System for the monthly average outputs (not shown). Model biases include a tendency to simulate a slightly weaker SST anomaly variability than the observations and a cooler mean SST in the model (by ~1°C). The comparison between model and observation for SST, thermocline and sea level is summarized in Table 1. Comparison of model vertical zonal current (anomalies) and Acoustic Doppler Current Profiler measurements from TAO indicates that the model also realistically simulates the zonal circulation (see Table 2). This simulation was used in a recent study to derive an estimate of the intraseasonal equatorial Kelvin wave over 2000–2008 [*Dewitte et al*., 2011].

Table 1. Validation of MERCATOR Along the Equator Over 2000–2008: Zonally Averaged (Between 140°E and 80°W) Correlation and RMS Error Between Model Outputs and Observations for SST Anomalies (TMI), the 20°C Isotherm Depth Anomalies (TAO Data) and Sea Level High Anomaly (TPJ Data)

	TMI -MERC (SSTA)	TAO-MERC (D20A)	TPJ-MERC (SLHA)
Mean correlation	0.7	0.76	0.81
Mean RMS error	0.75°C	10.2 m	3.53 cm

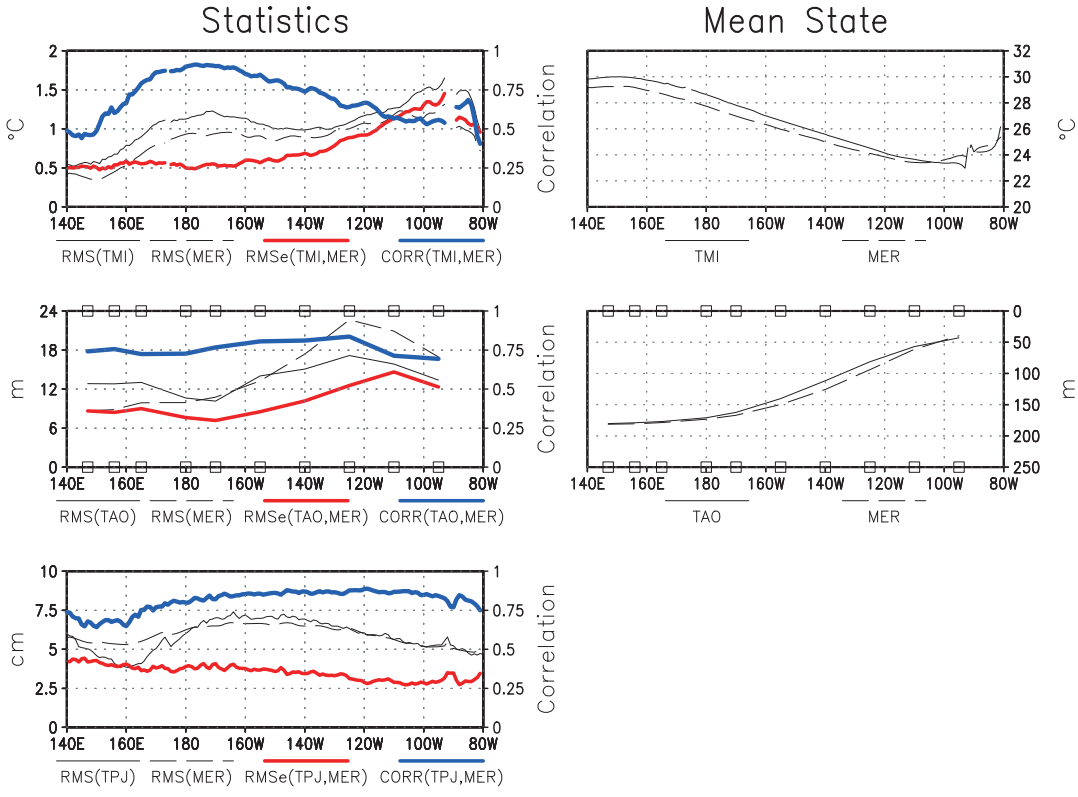

Figure 2. Comparison between model and observations. Left panels show the statistics for the anomaly of SST (upper), 20°C isotherm depth (center) and sea level high (SLH, bottom). In this side, each panel indicates the RMS of observed data, RMS of model results, RMS error (RMSe), and correlation (both between observed data and model results) using black solid line, black dashed line, red thick solid line, and blue thick solid line, respectively. The scale of RMS and RMSe is located on the left and correlation scale is on the right of each graphics. On the right-hand side, the mean SST (upper panel) and 20°C isotherm depth (lower panel) along the equator in 2000–2008 for model (dashed line) and observation (plain line). Open squares in the upper and lower borders of the panels indicate the position of the TAO mooring buoys in the equatorial line.

Table 2. Validation of MERCATOR Along the Equator Over 2000–2008 for Zonal Current Anomalies: Vertically Averaged (Between 0 and 55 m) Correlation and RMS Error Between Model Outputs and Observations. Observations are From the TAO Array

Mooring Longitude	165°E	170°W	140°W	110°W
Mean correlation	0.61	0.67	0.59	0.54
Mean RMS error (cm/s)	17.0	16.6	20.9	20.1

2.5. Estimation of Wave Amplitude

[9] To derive the Kelvin wave amplitude for the most energetic baroclinic modes ($m = 1$, 2 and 3), a similar methodology to that described in *Dewitte et al*. [2003] is used. It consists in projecting the variability on the vertical (baroclinic) and horizontal (Kelvin and Rossby) modes as obtained from the vertical mode decomposition of the mean stratification over the period 2000–2008. Usually wave amplitude is considered as its contribution to sea level or zonal current anomalies. Here, to compare with observed thermocline fluctuations as derived from the TAO data, we consider the Kelvin and Rossby wave contributions to thermocline anomalies following *Dewitte et al*. [2012], namely considering the vertical isotherm displacements at the depth of the mean thermocline under the hydrostatic approximation. The details of the method can be found in *Dewitte et al*. [2012].

3. Results

3.1. Equatorial Wave Sequence in July 2001 to October 2003

[10] As a first step, the contribution of the n^{th} baroclinic mode Kelvin (AK_n), first-meridional Rossby wave ($R1_n$) and third meridional Rossby wave ($R3_n$) to thermocline depth anomalies are estimated (see section 2.5). Figure 3b presents the evolution of the summed-up contribution of the Kelvin and first-meridional Rossby waves to thermocline fluctuations. The contribution of the first three baroclinic modes is considered here. Figure 3c is equivalent to Figure 3b except that only the contribution of the Kelvin wave is considered. They can be compared to Figure 3a, which displays the TAO observations. It first indicates that the thermocline variability along the equator can be accounted for to a large extent by the summed-up contribution of the Kelvin waves of the first three baroclinic modes (Figure 3c) since the level of agreement between observations and Kelvin wave estimate in terms of

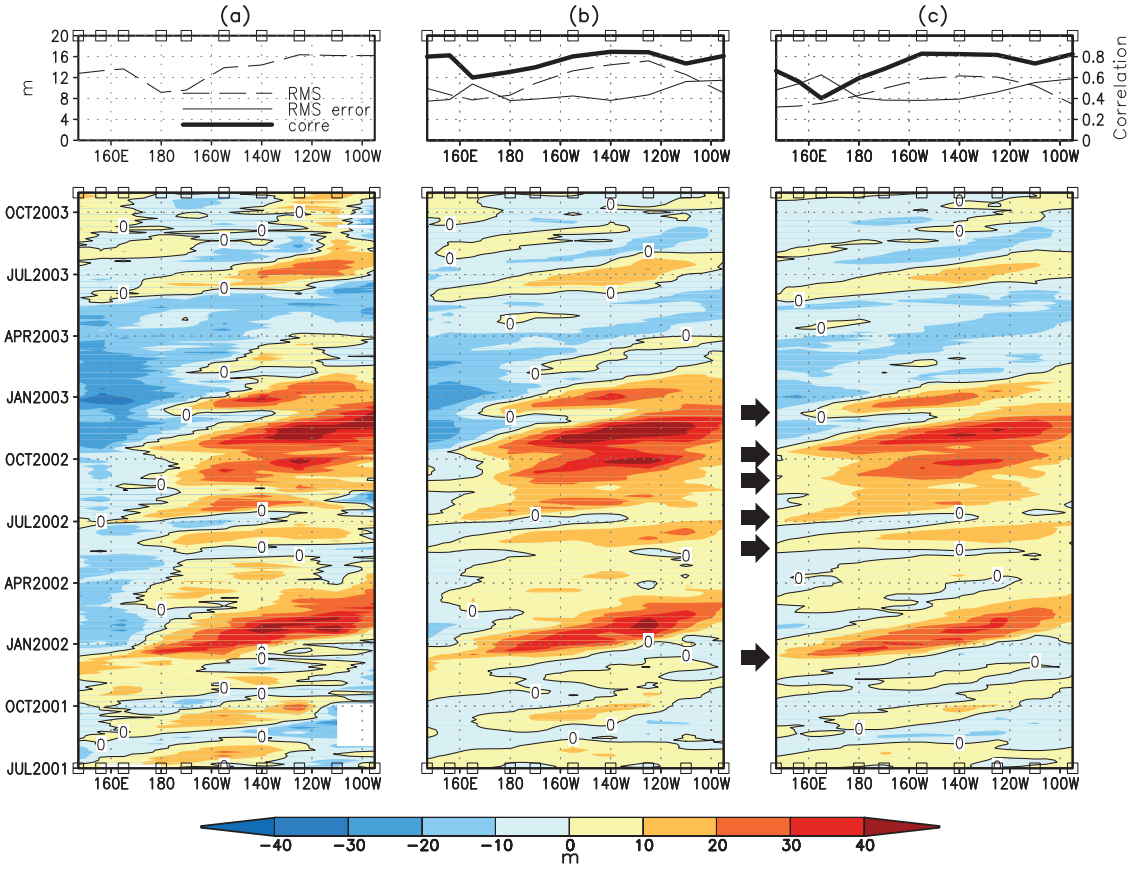

Figure 3. Evolution of thermocline depth anomalies along the equator between July 2001 and October 2003 (a) for the TAO data, (b) the contribution of the Kelvin and Rossby waves of the first three baroclinic modes, and (c) for the Kelvin wave contribution. Upper panels indicate the RMS (dashed line), RMS error (solid line), and correlation (thick solid line) between model and observation. Open squares in the superior axis of each graphic indicate the position of the TAO mooring buoys along the equator line. In Figure 3c, black arrows have been drawn to show the time of initiation of the downwelling Kelvin waves.

correlation and RMS error is comparable than for the total model thermocline anomalies (compare top Figure 3 with the left-center panel of Figure 2). Rossby waves contribute to the thermocline fluctuations mostly in the far western Pacific, but their contribution is more clearly seen around 4°N and 4°S. The simulated Kelvin wave can be clearly identified: It propagates as far as to the eastern boundary with a slight decrease in amplitude as it approaches the eastern boundary. During the developing phase of the 2002/2003 El Niño, two main episodes of downwelling Kelvin wave activity can be observed: An energetic downwelling Kelvin wave in January 2002 and a packet of five downwelling Kelvin wave (DKW) between April 2002 and January 2003 (see Figure 3c). Each DKW is associated to a westerly wind burst that took place in the western Pacific (Figure 4a).

[11] To visualize and infer the advection processes associated to the waves, the SST anomalies have been overlaid in Figures 4b, 4c, and 4d and only the amplitude of the Kelvin wave larger than 10 m is contoured. At the end of 2001, a westerly wind burst triggered a DKW that projected onto the first two baroclinic modes (Figure 4a, 4b, and 4c). This wave crossed the equatorial Pacific deepening the thermocline depth and slightly dissipating as it reaches the eastern Pacific in the austral summer of 2002. This wave slightly increased the SST over the eastern equatorial Pacific (Figure 1c) and may have been trapped along the Ecuadorian and Peruvian coasts producing coastal positive SST anomalies (Figure 1d). Also, this Kelvin wave, along its trajectory, encounters a steeper thermocline (i.e., increased zonal stratification) which may result in reflections into intraseasonal Rossby waves [*Busalacchi and Cane*, 1988] as suggested by the evidenced by the westward propagating current anomalies associated to the first-meridional Rossby wave (Figure 4e). After that, between mid and end of 2002, five DKWs of the first two baroclinic modes, produced by westerly wind bursts, appear in the equatorial Pacific and depressed the thermocline depth. This wave packet participated to the development of the 2002/2003 El Niño. In the eastern Pacific, around 120°W–110°W in November–December 2002, a Kelvin wave of the third baroclinic mode appeared as a consequence of the sloping thermocline that may have induced modal dispersion. Additionally, these waves transferred

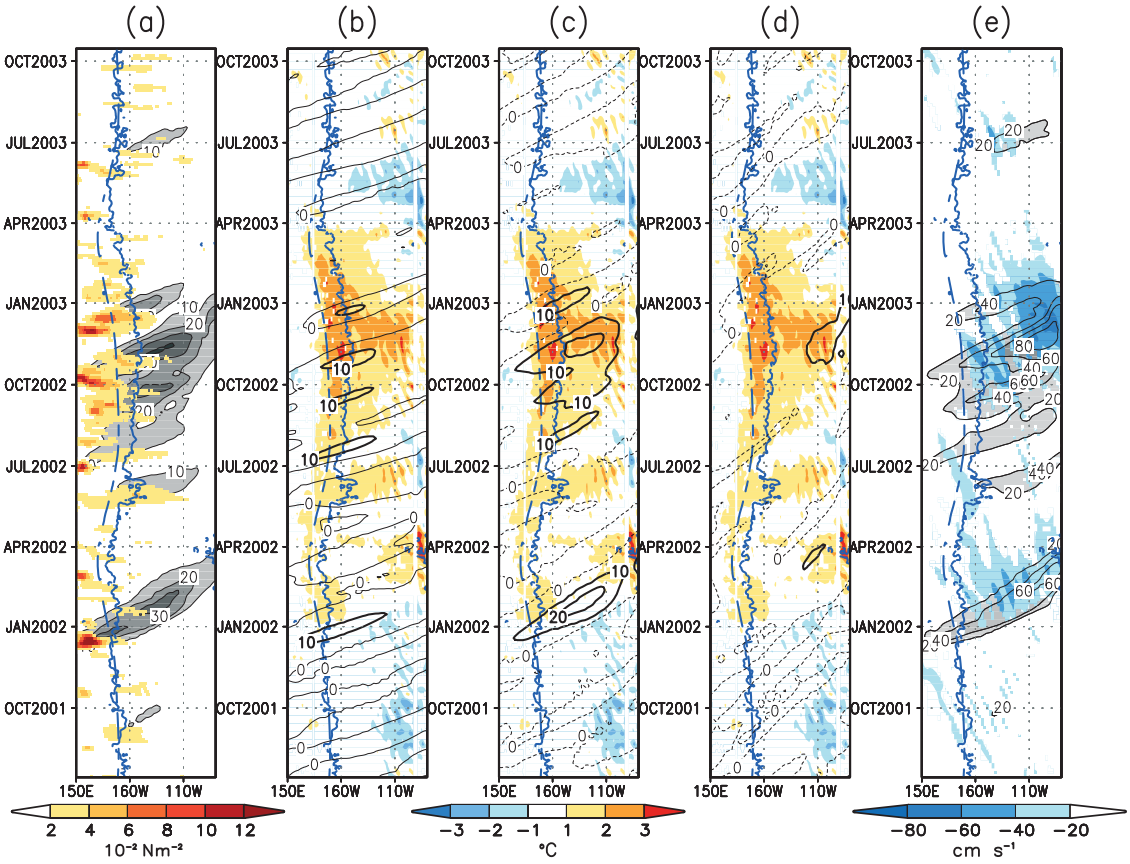

Figure 4. Evolution of equatorial zonal wind stress anomaly (ZWSA); the contribution of the Kelvin and Rossby waves to thermocline depth anomaly and zonal current anomaly, respectively; and SSTA along the equator line between July 2001 and October 2003. (a) Colors indicate the positive ZWSA (10^{-2} N m^{-2}) and gray scale, the contribution of DKW (sum of baroclinic modes 1, 2, and 3) (in meter). Shown in black lines are the contribution of the DKW from (b) mode 1, (c) mode 2, and (d) mode 3. In these three panels the SSTA from TMI is overlad in colors (scale is located at the bottom of Figure 4c). (e) The contribution of Kelvin and Rossby wave to the zonal current anomaly is drawn in black contours and in blue tones, respectively. The scale of the Rossby contribution is located at the bottom of Figure 4e. Also, the 28°C isotherm is overplotted in blue line for the climatological SST (dashed line) and the total SST (solid line) in all panels.

energy to the Rossby waves along their ways, eventually reflecting at the American boundary (Figure 4e). Note the slight eastward displacement of the warm pool associated to this wave packet (see the eastern movement of the 28°C isotherm—blue dashed line—in Figure 4), which indicates that the large-scale ocean-atmosphere feedbacks have fully engaged to amplify and sustain the CP El Niño warming. From January 2003, the Kelvin wave activity subsides and SST anomalies started to decrease and the 28°C isotherm reached its normal position around April of 2003.

3.2. Warming and Cooling Processes

[12] To document the processes at work during this CP El Niño event, a simplified heat budget model of a fixed depth layer ($h = 50$ m) is carried out from the MERCATOR data. The use of a constant depth is appropriate for estimating processes associated to wave dynamics in the equatorial Pacific and has been used in many ENSO studies (see *Zebiak and Cane* [1987] or *Belmadani et al*. [2010] among others). It is based on the following temperature anomaly equation:

$$\left\langle \frac{\partial T_A}{\partial t} \right\rangle_h = -\langle \mathbf{V}_A \cdot \nabla T_C \rangle_h - \langle \mathbf{V}_C \cdot \nabla T_A \rangle_h - \langle \mathbf{V}_A \cdot \nabla T_A \rangle_h + F_A + R \quad (1)$$

where $\langle X \rangle_h$ indicates the vertical average of the quantity X from the surface to the depth h, taken constant equal to 50 m. Subscript C and A, in some variables, represent climatology and anomaly, respectively. T, $\mathbf{V} = (u,v,w)$ and F are the temperature, velocity, and surface energy fluxes, respectively. The left-hand side term of equation (1) represents the tendency of T_A. On the right, the three advection terms, correspond to the combination of climatological and anomalous currents and gradients. The surface fluxes anomaly is estimated following *Wang and McPhaden* [1999], namely $F_A = (Q_0 + Q_P)/(\rho_0 C_p |h|)$, where Q_0 is the sum of anomalies of shortwave radiation (Q_{SW}), longwave radiation (Q_{LW}), latent heat (Q_L), and sensible heat (Q_S) (i.e., $Q_0 = Q_{SW} + Q_{LW} + Q_L + Q_S$), while Q_P is the outgoing shortwave fluxes that escape from the bottom of the layer: $Q_P = -0.45 \cdot Q_{SW} \cdot e^{-\gamma|h|}$. C_p, is the heat capacity (=3940 J kg^{-1} °C^{-1}), ρ_0 is the density of the seawater (=1022.4 kg m^{-3}) and $\gamma^{-1} = 25$ m is the attenuation length scale. Finally, R is the residual of the budget that includes physical processes such as vertical diffusion or entrainment.

[13] To estimate the role of the equatorial Kelvin waves on the rate of SST change during the evolution of the 2002/2003 El Niño, the contribution to zonal current anomalies is separated into its baroclinic component and a residual component calculated by the difference between total zonal current anomalies and the summed-up contribution of the baroclinic modes 1 to 3. This residual component therefore stands for the share of the variability that tends to be trapped into the fixed-depth mixed layer and accounts for the so-called locally wind-driven current anomalies along the equator. Such contribution could be also estimated considering a simple frictional layer of depth h forced by $\boldsymbol{\tau}_f = \boldsymbol{\tau}([1/h] - \sum_{i=1}^{3} P_i)$ [cf. *Blumenthal and Cane*, 1989] (P_i being the wind projection coefficient for the baroclinic mode i). As a consistency check, we have fitted such a frictional layer model so that residual component of the current, which leads to an estimation of the damping rate coefficient of ~(6 days)$^{-1}$. Although such estimated decay time is somewhat larger than what is usually used in intermediate complexity models [*Zebiak and Cane*, 1987], it is consistent with the interpretation of the residual component of the current anomalies as the locally wind-driven contribution.

[14] Equation (1) then writes as follows:

$$\begin{aligned} \frac{\partial T_A}{\partial t} = & -u_K \frac{\partial T_C}{\partial x} - u_R \frac{\partial T_C}{\partial x} - u_r \frac{\partial T_C}{\partial x} - v_A \frac{\partial T_C}{\partial y} - w_A \frac{\partial T_C}{\partial z} \\ & - u_C \frac{\partial T_A}{\partial x} - v_C \frac{\partial T_A}{\partial y} - w_C \frac{\partial T_A}{\partial z} \\ & - u_K \frac{\partial T_A}{\partial x} - u_R \frac{\partial T_A}{\partial x} - u_r \frac{\partial T_A}{\partial x} - v_A \frac{\partial T_A}{\partial y} - w_A \frac{\partial T_A}{\partial z} \\ & + \frac{Q_{SW}}{\rho_0 C_p h} + \frac{Q_{LW}}{\rho_0 C_p h} + \frac{Q_L}{\rho_0 C_p h} + \frac{Q_S}{\rho_0 C_p h} + \frac{Q_P}{\rho_0 C_p h} \\ & + R \end{aligned} \quad (2)$$

where u_K (u_R) is the contribution of the Kelvin (first and third meridional Rossby) wave, from the first three gravest baroclinic modes, to the zonal currents anomaly. Term u_r is the difference between u_A (total zonal current anomaly) and ($u_K + u_R$). Angle brackets ($< >_h$) has been omitted for clarity. Hereafter, each term are considered as its average within the layer h.

[15] Figure 5 displays the tendency terms of equation (1), as Hovmöller diagrams, over the period from July 2001 to October 2003 along the equator. The rate of SST changes (Figure 5a) clearly shows a warming and a cooling phase between April 2002 and November 2002, and December 2002 and April 2003, respectively. Advection (Figure 5b) is the most important process contributing to the warming of the 2002/2003 El Niño. It is partly compensated by surface flux anomalies (Figure 5c) that act as a thermal damping especially during the decaying phase of the event. The residual term (Figure 5d) does not exhibit a clear pattern. Its variability is the largest in the eastern Pacific where vertical diffusion and entrainment are likely to play a role due to the shallow fixed-depth mixed layer. Note however that the offline computation (based on 3 day mean averages of model variables) is not adequate for clearly separating entrainment and vertical mixing processes. What should appear as diurnal entrainment, for instance, appears in the offline computation as daily-mean vertical mixing. Anyway by construction our budget is closed. Only the interpretation of the physical process is limited in the eastern Pacific. With this limitation in mind, the following provides a description of the warming and cooling phases of the 2002/2003 El Niño in three equatorial regions having the zonal extent of the historical El Niño indices, namely N4Eq (160°E–150°W; 0°), N34Eq (170°W–120°W; 0°) and N3Eq (150°W–90°W; 0°). The periods of the warming and cooling phases are inferred from Figure 5a, i.e., April–November 2002 and December 2002 to April 2003, respectively.

3.2.1. Warming Phase

[16] Figure 6 displays the values of the tendency terms in the three regions along the equator during the warming phase. A contrasted situation between N3Eq and N4Eq is observed. In the central Pacific (N4Eq), the warming during the 2002/2003 El Niño is produced mainly by the zonal advection of the climatological temperature due to the Kelvin

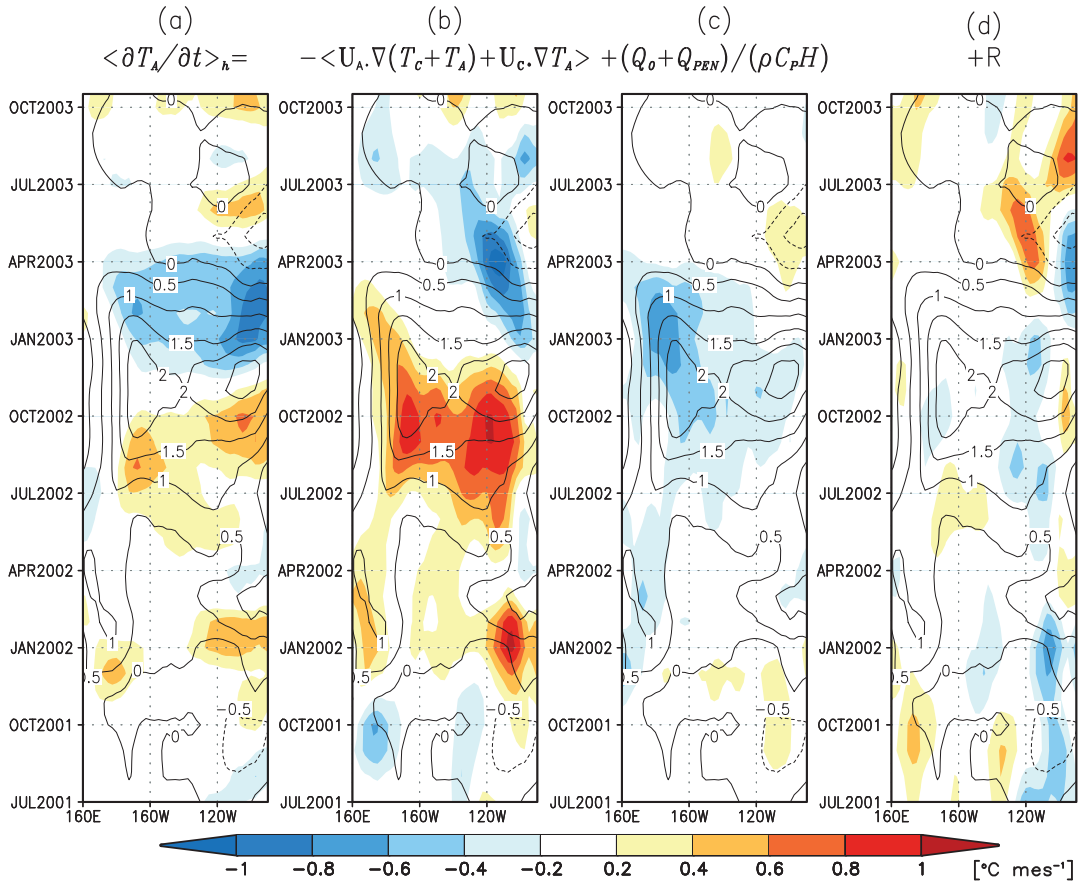

Figure 5. Evolution of the tendency terms (in colors) along the equator as defined in equation (1). (a) The rate of SST changes ($< \partial T_A/\partial t >_h$). (b) The advection terms, which means the sum of the first three terms on the right-hand side of equation (1). (c) The surface fluxes [fourth term of equation (1)]. (d) The residual term (R') that accounts for vertical mixing or entrainment. In each panel the SSTA is overlaid in black contours.

waves ($-u_K(\partial T_c/\partial x)$) and due to the locally wind-driven currents ($-u_r(\partial T_c/\partial x)$) whereas in the eastern Pacific (N3Eq), it is associated to the zonal advection of the climatological temperature due to the Kelvin waves ($-u_K(\partial T_c/\partial x)$) and the vertical advection of the temperature anomaly by climatology vertical velocity $-w_C(\partial T_A/\partial z)$. Consistently with Figure 4, the peak contribution of the zonal advection due to the Kelvin wave is found in the N34Eq region. Cooling processes during this warming phase are attributed to the Rossby wave component of the zonal advection term all along the equator (peaking in the N34Eq region) and to short wave radiation and latent heat in the N4Eq and N3Eq regions respectively. This is consistent with the increased convection in the N4 and the expected increased convergence east of it (N34Eq and N3Eq regions) during the warming of the warm pool. The residual term consists in a cooling tendency in the eastern Pacific which may be due to either the increase in vertical mixing at the crossing of the downwelling Kelvin wave or the unusual zonal extent of anomalous easterly stresses during this event [cf. *McPhaden*, 2004, Figure 5b].

3.2.2. Cooling Phase

[17] The cooling phase is associated to a different balance between terms (Figure 7) with in particular an enhanced contribution of the heat-flux damping through solar radiation reduction in the central Pacific (N4Eq) and increased evaporation along the equator (peaking in the N34Eq region). The zonal advection remains a major contributor to the rate of SST change, but mainly through its baroclinic component. The latter corresponds to the effect of the reflected downwelling Rossby waves that produces a cooling tendency in the N34Eq and N3Eq regions and the small warming tendency in the N4Eq region as a consequence of upwelling Rossby waves that, due to its zonal current structure at the equator, advect warm water from the western Pacific.

4. Discussion and Conclusions

[18] The 2002/2003 El Niño is characterized by SST anomalies developing and peaking in the central Pacific and a slight warming of the eastern Pacific. It is shown here that this event was associated to intraseasonal downwelling Kelvin wave activity of the first two baroclinic modes: a first downwelling Kelvin wave initiated ~8–9 month prior to the development of the CP El Niño that slightly warmed the equatorial Pacific and may have contributed to set up favorable conditions for its development; a second episode of downwelling Kelvin waves is diagnosed that occurred during the development phase from October 2002. These waves exhibit

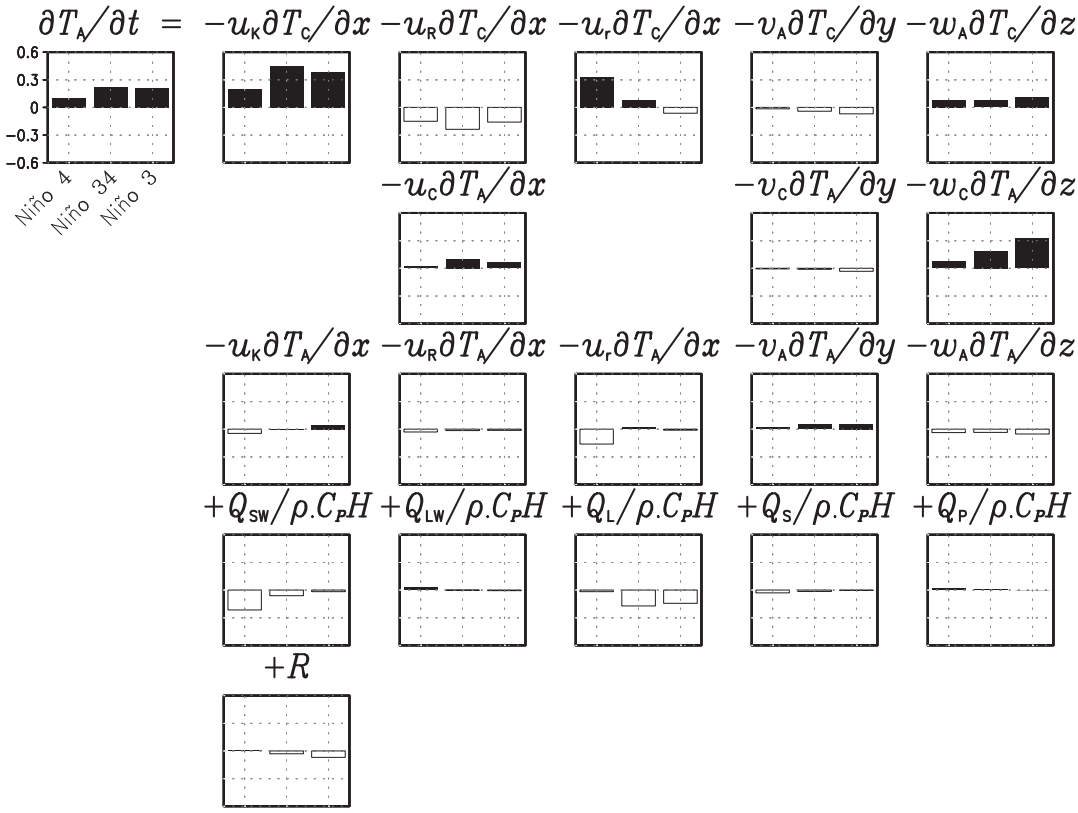

Figure 6. Three-bar plots for each term of equation (2) in the warming phase (April–November 2002) of 2002/2003 El Niño. The three bars indicate the mean value in regions El Niño 4 (left), El Niño 3.4 (center) and El Niño 3 (right); see text for the definition of regions. Filled (no filled) bar represents warming (cooling) contribution (°C month^{-1}).

a peak variability in the central Pacific, most prominent in the second baroclinic mode, and dissipate as they propagate eastward suggesting either vertical propagation, modal dispersion associated to the sloping thermocline from west to east, or mixing.

[19] A simplified heat budget analysis inside a fixed depth layer reveals that anomalous zonal advection of mean temperature and mean vertical advection of temperature anomaly are the major contributors to SST changes during the warming phase (April–November 2002), whereas the reversal toward cooler conditions (December 2002 to April 2003) is associated to zonal advection and net heat flux reduction. The zonal advection is further decomposed into a baroclinic component and a locally forced component trapped into the fixed-depth mixed layer. The latter reveals that the warming process in the central and eastern Pacific can be attributed to a large extent to the Kelvin waves. In the N4Eq region, it contributes as much as the direct wind forcing component to the zonal advection. Its effect in the eastern Pacific is enhanced by the contribution of the vertical advection. However there is a compensation by the latent heat and the vertical mixing, which may explain why SST anomalies in the N3Eq region do not exceed those in the N4Eq region. Noteworthy, there is a contribution of the Rossby waves to the zonal advection along the equator, which is apparently due to reflection of the Kelvin wave on the sloping thermocline. As a summary of the waves' sequence and their impact on advection, we provide a schematic of the evolution of the 2002/2003 El Niño (Figure 8).

[20] We now discuss our results in the light of previous works. Our analysis is overall consistent with the study by *Kug et al*. [2010] who analyzed a composite CP El Niño event as simulated by a Coupled General Circulation Model, in the sense that the zonal advection process is a dominant process to explain the development of the 2002/2003 El Niño whereas thermal damping is a major contributor to the "discharge process." Our results, however, suggest that there is a clear dynamical response in terms of equatorial wave, which does not rule out that processes relevant for the EP El Niño take place, which includes the recharge-discharge process [*Jin*, 1997]. In particular, *Dewitte et al*. [2012] showed that in the same OGCM simulation studied by *Kug et al*. [2010] that the recharge-discharge process could take place through the second baroclinic mode. Here we also find that different waves can have a different contribution to the evolution of heat content along the equator. However, conversely to the composite CP El Niño described in *Dewitte et al*. [2012], for the 2002/2003 El Niño, both baroclinic modes appear to contribute distinctively to the recharge and discharge processes. As an illustration, Figure 9 shows the evolution of the Warm Water Volume (WWV) anomaly for the contribution of the first and second baroclinic modes, for their summed-up contributions and the total field. The WWV is calculated following *Meinen and McPhaden* [2000]. Besides confirming the good agreement between the model used in this study and observations in terms of heat content anomalies, Figure 9 indicates that the

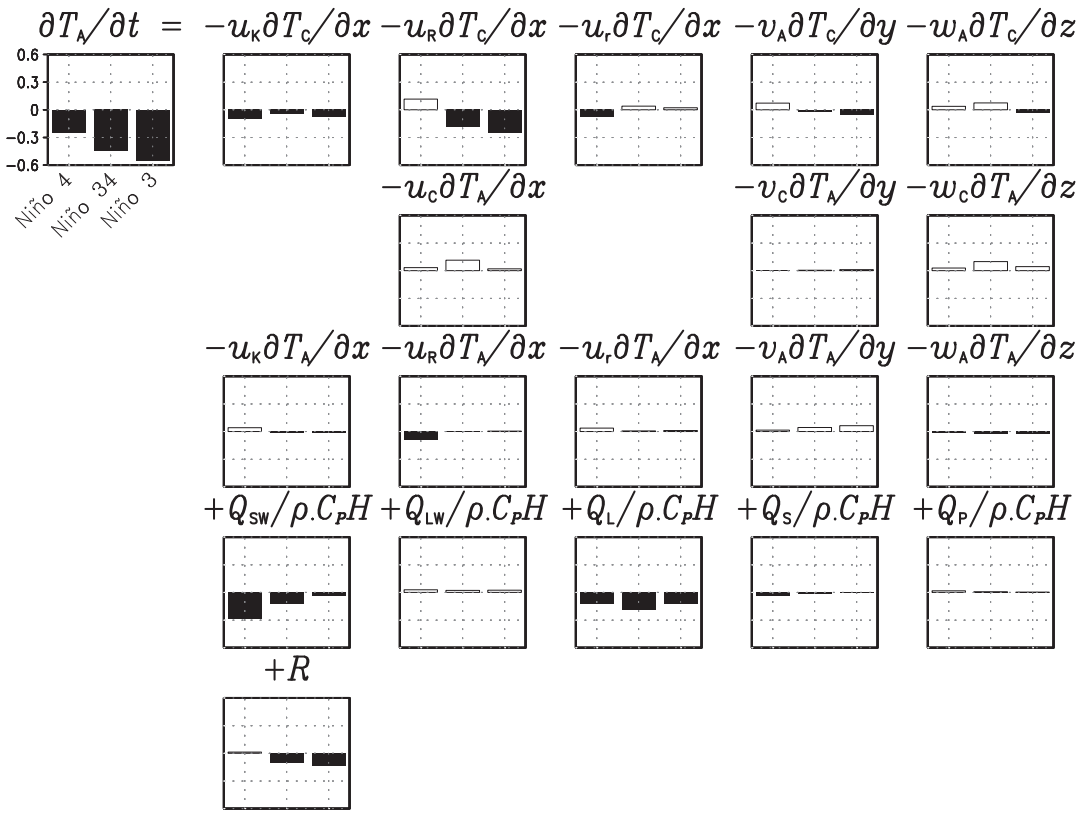

Figure 7. Similar to Figure 6 but for cooling phase (December 2002 to April 2003) of 2002/2003 El Niño. In contrast, filled (no filled) bar represents cooling (warming) contribution (°C month^{-1}).

second mode contributes to the recharge process whereas the first mode remains weak during this phase. After the peak phase (vertical dashed line) right after the peak SST anomaly, both modes experience a sharp decrease initiating the discharge process. The temporal integral of the first baroclinic mode contribution to the WWV anomaly over the cooling phase leads a negative value conversely to the second baroclinic mode, indicating that the first mode is dominating the discharge process. This suggests that there is a dynamical asymmetry between the recharge and discharge processes during the 2002/2003 El Niño with the second baroclinic mode contributing mostly to the recharge process and

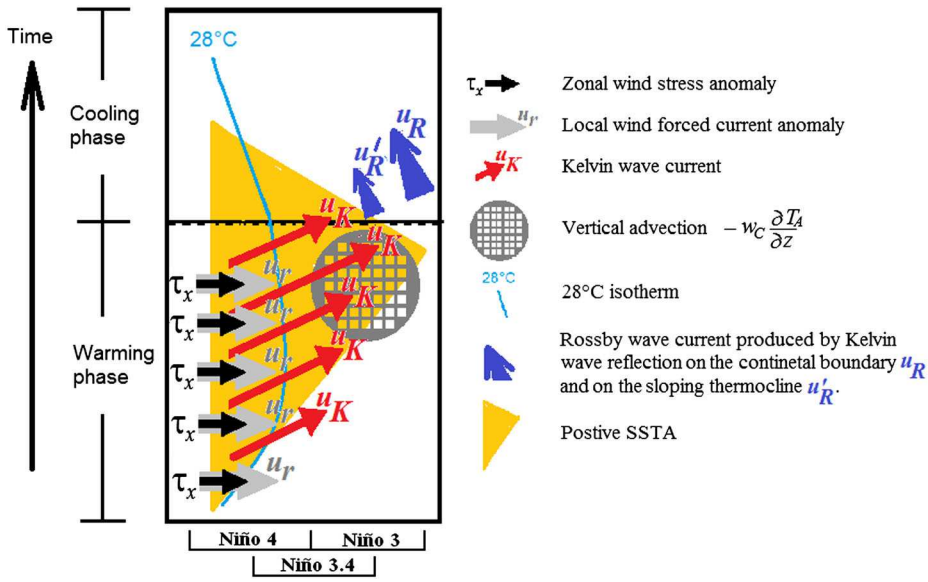

Figure 8. Schematic from derived results of the wave sequence and their impact on advection during the warming and cooling phases of the 2002/2003 El Niño along the equator.

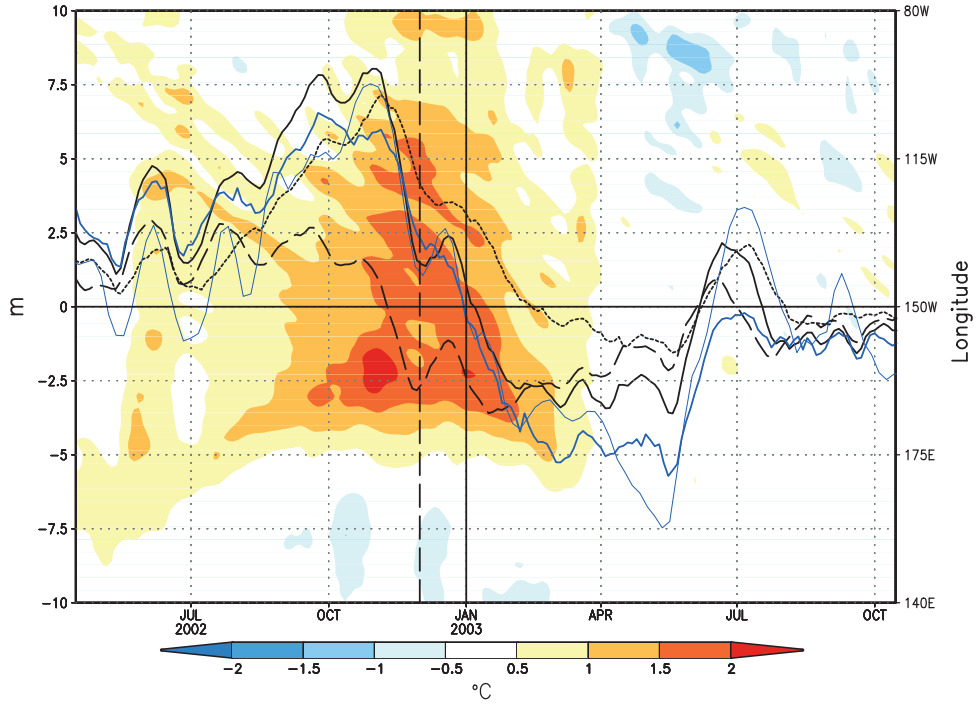

Figure 9. Evolution of the Warm Water Volume (WWV) as derived from TAO (thin blue line) and MERCATOR (thick blue line) between April 2002 and October 2003. The WWV is calculated from the spatial average of the 20°C isotherm depth anomaly over (145°E–95°E; 5°S–5°N) for TAO and (135°E–80°W; 5°S–5°N) for MERCATOR. The lines, in black, represent the contribution to the WWV of the sum of Kelvin and first meridional Rossby modes of the first two baroclinic modes. Dashed (dotted) line represents the first (second) baroclinic mode's contribution. The sum of vertical mode 1 and 2 is represented by a solid black line. As a background, the SSTA along the equatorial Pacific (mean over 5°S–5°N) is displayed (zonal axis is put on the right). Vertical dashed line indicates 1 December 2002, which is the limit between warming and cooling phase based in the tendency of SSTA (Figure 5).

the first baroclinic mode mostly amplifying the decay of the event. Because ENSO is sensitive to the thermocline depth and stratification [*Fedorov and Philander*, 2001], we may argue that such feature results from changes in stratification considering that the latter has been reduced during the last decade [*McPhaden et al*., 2011]. Further investigation is required in order to document if such dynamical asymmetry pattern in the evolution of the WWV is a fundamental characteristic of the CP El Niño and may explain recent changes in the relationship between WWV anomalies and SST anomalies at the peak phase of ENSO [*McPhaden*, 2012].

[21] Our study also indicates that vertical mixing, taken into account here as a residual term (*R*'), also participates in the compensation of the effect of the Kelvin wave onto the vertical advection, which may explain the evolution of this event toward a CP type. Further investigation is required in order to separate the contribution of the different terms participating to vertical mixing, that is vertical diffusivity and entrainment. This can be achieved through an online computation of the heat budget, which we plan to do from another OGCM. In particular, *Lengaigne et al.* [2012] indicates that vertical mixing can significantly contribute to the WWV tendency during the 2002/2003 El Niño [see *Lengaigne et al*., 2012, Figure 8]. This contribution as well as the one from the penetration solar forcing at the 20°C isotherm depth may explain the differences that we find between the total WWV and the estimate from the Kelvin and first meridional Rossby waves (summed-up of baroclinic modes 1 and 2) at the peak phases of the recharge and discharge (Figure 9). Our results indicate however that the main contribution to the WWV tendency originates from the wave dynamics, which is consistent with the results by *Bosc and Delcroix* [2008]. This suggests that, despite its weak amplitude, the CP El Niño may be as predictable as the EP El Niño, even though a modulation of the predictability may originate from change in mean state [*McPhaden et al*., 2011]. Further study is certainly required to document the wave dynamics of such type of event to determine if the dynamical vertical structure of the WWV could explain the reduced seasonal time scale predictability during periods dominated by CP El Niños.

[22] **Acknowledgments.** K. Mosquera-Vásquez benefited from a Ph. D. scholarship received from Institut de Recherche pour le Développement (IRD). The authors also thank the two anonymous reviewers for their constructive comments. This work is part of the projects of the special agreement between IRD and IGP (2011–2013).

References

Ashok, K., S. K. Behera, S. A. Rao, H. Weng, and T. Yamagata (2007), El Niño Modoki and its possible teleconnection, *J. Geophys. Res.*, *112*, C11007, doi:10.1029/2006JC003798.

Belmadani A., B. Dewitte, and S.-I. An (2010), ENSO feedbacks and associated variability timescales in a multi-model ensemble, *J. Climate*, *23*, 3181–3204.

Bosc, C., and T. Delcroix (2008), Observed equatorial Rossby waves and ENSO-related warm water volume changes in the equatorial Pacific Ocean, *J. Geophys. Res.*, *113*, C06003, doi:10.1029/2007JC004613.

Blumenthal, M. B., and M. A. Cane (1989), Accounting for parameter uncertainties in model verification: An illustration with tropical sea surface temperature, *J. Phys. Oceanogr.*, *19*, 815–830.

Busalacchi, A. J., and M. A. Cane (1988), The effect of varying stratification on low-frequency equatorial motions, *J. Phys. Oceanogr.*, *18*, 801–812.

Chelton, D. B., S. K. Esbensen, M. G. Schlax, N. Thum, M. H. Freilich, F. J. Wentz, C. L. Gentemann, M. J. McPhaden, and P. S. Schopf (2001), Observations of coupling between surface wind stress and sea surface temperature in the eastern tropical Pacific, *J. Clim.*, *14*, 1479–1498.

Clarke, A. J., and C. Shi (1991), Critical frequencies at ocean boundaries, *J. Geophys. Res.*, *96*, 10,731–10,738.

Dewitte B., S. Illig, L. Parent, Y. duPenhoat, L. Gourdeau, and J. Verron (2003), Tropical Pacific baroclinic mode contribution and associated long waves for the 1994–1999 period from an assimilation experiment with altimetric data, *J. Geophys. Res.*, *108* (C4), 3121–3138.

Dewitte B., S. Illig, L. Renault, K. Goubanova, K. Takahashi, D. Gushchina, K. Mosquera, and S. Purca (2011), Modes of covariability between sea surface temperature and wind stress intraseasonal anomalies along the coast of Peru from satellite observations (2000–2008), *J. Geophys. Res.*, *116*, C04028, doi:10.1029/2010JC006495.

Dewitte B., J. Choi, S.-I. An, and S. Thual (2012), Vertical structure variability and equatorial waves during central Pacific and eastern Pacific El Niños in a coupled general circulation model, *Clim. Dyn.*, *38*, 2275–2289.

Ducet, N., P. Y. Le Traon, and G. Reverdin (2000), Global high resolution mapping of ocean circulation from TOPEX/POSEIDON and ERS-1/2, *J. Geophys. Res.*, *105*, 19,477–19,498.

Fedorov, A. V., and S. G. Philander (2001), A Stability Analysis of Tropical Ocean–Atmosphere Interactions: Bridging Measurements and Theory for El Niño, *J. Clim.*, *14*, 3086–3101.

Fu, L.-L., E. J. Christensen, C. A. Yamarone Jr., M. Lefebvre, Y. Menard, M. Dorrer, and P. Escudier (1994), Topex/Poseidon mission overview, *J. Geophys. Res.*, *99*, 24,369–24,381.

Garric G., R. Bourdalle-Badie, O. Le Galloudec, C. Bricaud, C. Derval, E. Durand, and Y. Drillet (2008), Description of the interannual experiment ORCA025-T09, 1998–2006, Mercator Ocean Report n°235, September 2008.

Gentemann, C. L., C. J. Donlon, A. Stuart-Menteth, and F. J. Wentz (2003), Diurnal signals in satellite sea surface temperature measurements, *Geophys. Res. Lett.*, *30*(3), 1140, doi:10.1029/2002GL016291.

Hayes, S. P., P. Chang, and M. J. McPhaden (1991), Variability of the sea surface temperature in the eastern equatorial Pacific during 1986–88, *J. Geophys. Res.*, *96*, 10,553–10,566.

Jin, F.-F. (1997), An equatorial ocean recharge paradigm for ENSO. Part I: conceptual model, *J. Atmos. Sci.*, *54*, 811–829.

Kim, W., S.-W. Yeh, J.-H. Kim, J.-S. Kug, and M. Kwon (2011), The unique 2009–2010 El Niño event: A fast phase transition of warm pool El Niño to La Niña, *Geophys. Res. Lett.*, *38*, L15809, doi:10.1029/2011GL048521.

Kug, J.-S., F.-F. Jin, and S.-I. An (2009), Two types of El Niño events: cold tongue El Niño and warm pool El Niño, *J. Clim.*, *22*, 1499–1515.

Kug, J.-S., J. Choi, S.-I. An, F.-F. Jin, and A. T. Wittenberg (2010), Warm Pool and Cold Tongue El Niño events as simulated by the GFDL 2.1 coupled GCM, *J. Clim.*, *23*, 1226–1239.

Le Traon, P. Y., and F. Ogor (1998), ERS-1/2 orbit improvement using T/P: the 2 cm challenge, *J. Geophys. Res.*, *103*, 8045–8057.

Lee, T., and M. J. McPhaden (2010), Increasing intensity of El Niño in the central-equatorial Pacific, *Geophys. Res. Lett.*, *37*, L14603, doi:10.1029/2010GL044007.

Lengaigne, M., U. Hausmann, G. Madec, C. Menkes, J. Vialard, and J. M. Molines (2012), Mechanisms controlling warm water volume interannual variations in the equatorial Pacific: diabatic versus adiabatic processes, *Clim. Dyn.*, *38*, 1031–1046.

Levitus, S., T. P. Boyer, M. E. Conkright, T. OBrian, J. I. Antonov, C. Stephens, L. Stathopolos, D. Johnson, and R. Gelfeld (1998), World Ocean Database 1998 - NOAA Atlas NESDID18, National Oceanographic Data Center, Silver Spring, MD.

Madec, G., P. Delecluse, M. Imbard, and C. Levy (1998), OPA 8.1 Ocean General Circulation Model reference manual, Nodes du pole de modélisation, Institut Pierre Simon Laplace (IPSL), France, 11, 91 pp.

McPhaden, M. J., et al. (1998), The Tropical Ocean-Global Atmosphere (TOGA) observing system: A decade of progress, *J. Geophys. Res.*, *103*, 14,169–14,240.

McPhaden, M. J. (2004), Evolution of the 2002/03 El Niño, *Bull. Am. Meteorol. Soc.*, *85*, 677–695.

McPhaden, M. J., T. Lee, and D. McClurg (2011), El Niño and its relationship to changing background conditions in the tropical Pacific, *Geophys. Res. Lett.*, *38*, L15709, doi:10.1029/2011GL048275.

McPhaden, M. J. (2012), A 21st Century Shift in the Relationship between ENSO SST and Warm Water Volume Anomalies, *Geophys. Res. Lett.*, *39*, L09706, doi:10.1029/2012GL051826.

Meinen, C. S., and M. J. McPhaden (2000), Observations of warm water volume changes in the equatorial Pacific and their relationship to El Niño and La Niña, *J. Clim.*, *13*, 3551–3559, doi:10.1175/1520-0442(2000)013 < 3551:OOWWVC > 2.0.CO;2.

Rayner, N. A., D. E. Parker, E. B. Horton, C. K. Folland, L. V. Alexander, D. P. Rowell, E. C. Kent, and A. Kaplan (2003), Global analyses of sea surface temperature, sea ice, and night marine air temperature since the late nineteenth century, *J. Geophys. Res.*, *108*(D14), 4407, doi:10.1029/2002JD002670.

Takahashi, K., A. Montecinos, K. Goubanova, and B. Dewitte (2011), ENSO regimes: Reinterpreting the canonical and Modoki El Niño, *Geophys. Res. Lett.*, *38*, L10704, doi:10.1029/2011GL047364.

Wang, W., and M. J. McPhaden (1999), The surface layer heat balance in the equatorial Pacific ocean. Part I: Mean seasonal cycle, *J. Phys. Oceanogr.*, *29*, 1812–1831.

Wentz, F. J., C. Gentemann, D. Smith, and D. Chelton (2000), Satellites measurements of sea surface temperature through clouds, *Science*, *288*, 847–850.

Yeh S.-W., S.-J. Kug, B. Dewitte, M.-H. Kwon, B. P. Kirtman, and F.-F. Jin (2009), El Niño in a changing climate, *Nature*, *461*, 511–514.

Yu, J.-Y., and S. T. Kim (2010), Three evolution patterns of Central Pacific El Niño, *Geophys. Res. Lett.*, *37*, L08706, doi:10.1029/2010GL042810.

Yu, J.-Y., H.-Y. Kao, T. Lee, and S. T. Kim (2011), Subsurface ocean temperature indices for Central-Pacific and Eastern-Pacific types of El Niño and La Niña events, Theoretical Appl. *Climatol.*, *103*, 337–344.

Zebiak, S. E., and M. A. Cane (1987), A model El Niño-Southern Oscillation, *Monthly Weather Review*, *115*, 2262–2278.